Enhanced aramid/Al2O3 interfacial properties by PDDA-modification for the preparation of composite insulating Paper

Fangcheng Lv
North China Electric Power University
Xiuquan Lu
North China Electric Power University
Jingxuan Song (jingxuan.song@foxmail.com)
North China Electric Power University
Meiying Zhu
North China Electric Power University
Shenghui Wang
North China Electric Power University
Yuqin Xu
North China Electric Power University
Xiaobin Chang
Ganzhou Longpont Material Technology Co., LTD

Research Article

Keywords: PMIA, PDDA, Nano-Al2O3, Interface characteristics, Insulation performance

Posted Date: June 17th, 2022

DOI: https://doi.org/10.21203/rs.3.rs-1742242/v1

Abstract

For further improve the electrical insulation properties of meta-aramid paper(PMIA), polydimethyldiallyl ammonium chloride (PDDA) was used for the modification of nano-Al_2O_3 in this work. The modified products were characterized by means of transmission electron microscopy (TEM), Fourier transform infrared spectrometer (FTIR) and liquid Zeta potential. The original and PDDA modified nano-Al_2O_3 was doped into the aramid fiber composite, and the effects of PDDA and filler mass fraction on several properties such as electrical conductivity, breakdown strength and surface charge dissipation rate of insulating paper were studied. Finally, the interfacial properties of the composites were investigated using molecular dynamics (MD). The results showed that PDDA was successfully coated on the surface of nano-Al_2O_3, and its surface potential was changed from negative to positive, which could improve the interface characteristics between filler and matrix and enhance the dielectric strength of aramid paper. Besides, saturation effect of PDDA modification was observed, and when the amount of PDDA was 10% and the content of modified nano-Al_2O_3 was 3%, the breakdown strength of aramid paper was increased by 20%, and the volume conductivity was decreased by 68%. The simulation result revealed that PDDA could improve the insulation performance of aramid paper by reducing the interfacial binding energy between aramid and filler.

1 Introduction

Meta-aramid fiber, (PMIA, poly(m-phenylene isophthalamide)), is a high-performance polymer fiber and its main molecular chain is composed of alternating series of benzene rings and amide groups.[1] As a new type of insulating material, PMIA possess high thermodynamic stability and dielectric strength, which make it an ideal substitute of traditional cellulose insulating paper for new energy power systems.[2] At present, the most popular meta-aramid fiber product on the market is the Nomex series insulating paper developed by DuPont (United States) with a temperature resistance of 180 ℃ and an electrical insulation strength of nearly 25 kV/mm. [3,4] Imported insulating paper was widely used in some important power transformation equipment carrying personal safety and economic benefits, such as mining transformers, high-speed railway traction transformers and urban distribution transformers. However, the high price and extremely poor cost performance hinder its application in new energy power systems, so it is necessary to enhance and improve its electrical insulation performance.

Nano-Al_2O_3 has very high specific surface area, small size effect and quantum effect,[5] which could strengthen the defect structure of polymer materials and generate composite products with better performance. The previous works have found that nano-Al_2O_3 have showed a certain effectiveness in the reinforcement of composites materials. The doping of nano-Al_2O_3 affects the properties, including the AC/DC breakdown,[6,7] partial discharge,[8] flashover,[9] electrical conductivity, [10,11] dielectric constant,[12] thermal conductivity,[13] and mechanical properties.[14] Other reports have exhibited that nano-Al_2O_3 could improve the breakdown,[15,16] electrical conductivity, aging and other properties of cellulose paper in the

transformer oil-paper insulation system.[17] The reasons can be attributed to the higher dielectric constant and outstanding properties of nano-Al_2O_3. The interaction between polymer chains was enhanced and a large number of deep traps which could store electrons were introduced, thereby inhibiting the transport of carriers in the composite material and reducing the accumulation of space charges. [18,19] Studies have shown that appropriate amount of nano-inorganic fillers could limit the carrier migration of aramid paper, introduce deep traps and improve the breakdown strength.[20] The modification mechanism could be explained from the perspective of interface stability. However, only a few types of fillers have been investigated and in-depth discussions on the interface, the key factor of modification, are still rare.

The interfacial characteristics between nanoparticles and matrix has a very significant influence on the electrical properties of composite materials.[21] However, due to the obvious variations in microstructure and physical and chemical parameters, the interfacial stability between polymers and inorganic fillers was often adversely affected and even the modification effect can be offset in some cases. Therefore, it is necessary to dispose the fillers with surface modifying agents, which could act both as "bridges" between nanoparticles and organic compounds and physical bonding, resulting in smooth transition of properties during the preparation of composite materials.[22] In addition, the surface treatment of nanofillers by coupling agents can reduce the surface bonding energy of particles and prevent the formation of hydrogen bonds between particles, thereby improving the dispersibility of fillers in the matrix.[23] Zhang et al. studied the modification effect of phthalate coupling agent. The surface hydrophobicity of the modified nanoparticles was effectively improved, which could inhibit the injection and movement of space charges.[24] In another work, the crystallinity nano-TiO_2 was improved by surface etching utilizing silane coupling agent, and epoxy resins with better insulating properties was achieved. [25] Kan et al. proposed a polymer-impregnated surface modification method based on the asperities and porous surface structure of the nanoparticle, which could improve the tensile properties of the composites.[26] The introduction of multiple functional groups with different activities and appropriate ratio to the surface of nanoparticles could reduce the aggregation and non-specific binding between particles, making it easier to combine with organic molecules.[27]

Poly dimethyl diallylammonium chloride (PDDA) is a common polycationic surface modification reagent, which can improve the performance of nanomaterials by means of producing physicochemical interactions between multifunctional long chains and nanofillers. Li et al. coated PDDA on the surface of nano-Fe3O4 by chemical co-precipitation. The Zeta potential of the synthesized composite material became positive and the particle size became smaller.[28] Ratajski et al found that PDDA as a surfactant could improve the retention and dispersion of silica in the matrix without damaging the original composite structure.[29] In addition, PDDA exhibits good dissociation ability in a wide range of pH in both water and ethanol.[30] It is foreseeable that PDDA has high applicability to the pulp environment during the papermaking process. However, to the best of our knowledge, only few reports are concerned about PDDA-modified aramid paper fillers.

In this paper, a series of modified nano-Al_2O_3 with different mass fractions of PDDA was synthesized and used as filler in the preparation of Al_2O_3/PMIA composite insulating paper via wet papermaking. The effect and reaction mechanism of cationic polymer-grafted nanoparticles were studied by comparing the physical, chemical properties and microstructure of nano-Al_2O_3 before and after modification. The conductivity, breakdown strength and trap properties of the samples were tested, and the effect mechanism of interface properties of PDDA on the Al_2O_3/PMIA was analyzed by MS simulation. This work may provide both theoretical basis and practical methods for the subsequent improvement of performance of aramid insulating paper and further research of other composite materials.

2 Experiment

2.1 | Materials

Meta-aramid chopped fiber and precipitating fiber, Ganzhou Longbang Material Technology Co., Ltd., the diameter of the precipitating fiber ranges from 100 nanometers to tens of micrometers, the diameter of the chopped fiber is around 10 μm and the section is flat and long; Nano-Al_2O_3 (α-Al_2O_3, with an average particle size of 30nm ,purity 99.99%, Shanghai Chaowei Nano Technology Co., Ltd.); Polyethylene oxide (PEO, Beijing Wantuming Technology Co., Ltd.); Poly(dimethyldiallylammonium chloride)(40 wt% aqueous solution, Mw 200,000-350,000, Cool Chemical Technology (Beijing) Co., Ltd); Ethanol (C_2H_6O, 99.99%, Jiangsu Biaohui Chemical Co., Ltd.); NaOH, (≥ 96%, Shanghai Aladdin Biochemical Technology Co., Ltd.);NaCl(AR Sinopharm Group Chemical Reagent Co., Ltd.)、 Deionized water, self-made ultrapure water machine.

2.2 | Experiment

1) PDDA pretreatment of Al_2O_3

1.5g nano-Al_2O_3 was mixed into 60g deionized water and stired for 10 min, then 10ml NaOH solution with a content of 0.5 mol/L was added, and the mixture was ultrasonically dispersed for 10 min, then hydroxylation for 0.5h at 60°C. PDDA aqueous solution with a content of 0.05 mol/L chlorinated Sodium was added according to different mass ratio, including 0%, 10%, 20%, 40%, 80%, and the mixture was ultrasonically dispersed for 5 min, then stirred for another 4 h in a sealed water bath at 80°C. Finally, the suspension liquid was filtered and washed three times with deionized water, dried in an 100°C oven for 8 h. The obtained modified Al_2O_3 powder was denoted as P-Al_2O_3.

2) Preparation of modified Al_2O_3/PMIA paper

PEO and ultrapure water were prepared into a PEO solution as a dispersant in a mass ratio of 1:2000, which was put into a plastic bucket for use. 2000ml ultrapure water and 130ml PEO aqueous solution was poured in a standard fiber disintegrating machine, and revolved 15,000 r at a speed of 3 000r/min. Then P-Al_2O_3 in different concentration were added, and continued to disperse for 30000 revolutions.

After that, 1.2g chopped and 2.8g precipitating fibers were added, and decompressed for 75,000 revolutions. Then a paper machine was used for suction filtration and sheet making, and the finished paper were flat on a heating plate. Finally, papers were dryed in vacuum environment at 110°C for 20 minutes to remove most of the water, and then the flat vulcanizer and chrome-plated mold were used for 3 times of hot pressing with the parameters of 270 ℃, 10 MPa, each time for 20s. The diameter of the aramid composite papers prepared by this process were 200 ± 2 mm and the thickness were 0.16 ± 0.02 mm, the quality loss during the period was less than 5%. The specific reagent dosage for each sample was shown in Table 1 and the specific process was displayed in Fig. 1.

Table 1
specific reagent dosages of Al_2O_3/PMIA sample

Item	PDDA concentration(wt%)	Nano Al_2O_3 concentration(wt%)	Fibrid(g)	Chopped fiber(g)
P-0	0	3	2.8	1.2
P-10	10	3	2.8	1.2
P-20	20	3	2.8	1.2
P-40	40	3	2.8	1.2
P-80	80	3	2.8	1.2
P-10/1	10	1	2.8	1.2
P-10/5	10	5	2.8	1.2
P-10/7	10	7	2.8	1.2

Figure 1 preparation process of Al_2O_3/PMIA paper

Table 1 specific reagent dosages of Al_2O_3/PMIA sample

2.3 | Characterization

The Zeta potential of nano-Al_2O_3 before and after modification in aqueous solution under neutral environment were studied by liquid Zeta particle potential analyzer (DLS, Zetasizer Nano S90). The chemical compositions of Al_2O_3, PDDA and P-Al_2O_3 composites were analyzed by Fourier transform infrared spectrometer (FTIR, Nicolet IS5) with wavenumbers ranging from 400 cm^{-1} to 4000 cm^{-1}. Field emission transmission electron microscopy (TEM, Tecnai G2 F20) was used to observe the morphology of Al_2O_3 before and after modification in water. The sample was obtained by dispersing the powder in deionized water to prepare a 0.15% dispersion, the carrier network was selected as an ultra-thin carbon film, the image was bright field image. The section of the aramid composite paper was characterized by

field emission scanning electron microscope (SEM, Quanta 250 FEG), The section obtained by brittle fracture in liquid nitrogen and treated with gold spraying. Thermogravimetric analyzer (TG-DSC, TA-Q600) was used to test the thermal decomposition weight loss of aramid paper during the process of raising the temperature from 20 to 800 ℃ at a heating rate of 10 K/min under nitrogen atmosphere.

3 Results And Discussion

3.1 | Characterization

(1) FTIR test:

The effect and mechanism of PDDA-modified Al_2O_3 were characterized by infrared spectroscopy (FTIR). The infrared spectra of PDDA, Al_2O_3 and P-Al_2O_3 were shown in Fig. 2(a). The broad peak at 3357 cm^{-1} in the infrared spectrum of PDDA belonged to the result of N-H stretching vibration. 2932 cm^{-1} and 1470 cm^{-1} were the peaks of C-H stretching vibration from methylene and C-H asymmetric deformation vibration from N-CH3. The absorption peak at 1638 cm^{-1} was attributed to the unsaturated C = C stretching vibration in the PDDA molecular chain; 1099 cm^{-1} was the C-N in-plane bending vibration. The -OH stretching vibration peak of Al_2O_3 near 3472cm^{-1} before modification belonged to the hydroxyl groups adsorbed on the surface of Al_2O_3. 642 cm^{-1} and 606 cm^{-1} were the bending vibration absorption peaks of Al-O. The absorption peak intensity corresponding to -OH decreased significantly in the PDDA-modified composite material, indicating the involvement of hydroxyl group in the reaction during the coating process. The absorption peak at 2922 cm^{-1} was attributed to the antisymmetric stretching vibrations of methyl and methylene on the PDDA polymer chain. The peak at 1622 cm^{-1} could be attributed to the vibration absorption peaks associated with C-C, C-N, and the presence of carbon nitrogen heterocycle, indicating the presence of PDDA in the composite. In addition, the characteristic peaks of P-Al_2O_3 shifted to low wavenumbers. According to the above analysis, it was proved that PDDA was successfully grafted on the surface of nano-Al_2O_3 by intermolecular hydrogen bonding and chemical bonding.

(2) Zeta potential test:

The Zeta potential of nano-Al_2O_3 modified with different PDDA concentrations was shown in Fig. 2(b). The surface potential of unmodified nano-Al_2O_3 was − 21.9 mV and the potential became positive after PDDA modification. The Zeta potential varied from 28.9 mV to 36.4 mV when the amount of PDDA was changed. When the amount was too high the zeta potential increased overall, but the distribution uniformity decreased to some extent. When the absolute value of the Zeta potential was greater than 30 mV, the particles had better dispersion and stability. This might indicate that the electrical properties of the modified surface were reversed. Considering that meta-aramid always exhibits negative zeta potential in aqueous solution, PDDA-modified nano-Al_2O_3 particles would be expected to achieve classical connection with aramid fibers, thereby improving the dispersion and stability of fillers in composites.

Figure 2 (a)FTIR comparion between PDDA, Al_2O_3 and PDDA/ Al_2O_3 nanocomposites. (b)Particle zeta potential of nanocomposites with PDDA concentration

(3) TEM

The transmission electron microscope (TEM) images of P-0, P-10 and P-80 at different magnifications were shown in Fig. 3. It could be seen from the comparison that the black part in Fig. 3 was the united nano-Al_2O_3 particles and the gray part was the PDDA shell. PDDA was successfully coated on the surface of the nano-Al_2O_3 particles, forming a core/shell structure. In Fig. 3(b), the composite filler had an irregular shape when the mass fraction of PDDA was 10%. After adding PDDA, it aggregated on the surface of individual particle to achieve the coating effect instead of capturing more particles at the same time. In Fig. 3(c), the amount continued to increase after which PDDA fell off from the surface of Al_2O_3 and the polymer chain self-polymerized, weakening the coating effect.

Figure 3 The TEM images of (a)P-0, (b)P-10, (c)P-80

According to the above microscopic characterization results, the reaction process of PDDA grafted modified Al_2O_3 was shown in Fig. 4. The alkaline environment promoted the adsorption of a large amount of OH- in the solution on the surface of nano-Al_2O_3, resulting in a negative surface potential. PDDA dissociated Cl- and positively charged polymer long molecular chains in the ethanol/water mixed solution. The hydrophilic amino groups provided the lone electron pairs, and the positively charged amino groups further combined with the hydroxyl groups on the surface of nano-Al_2O_3. New chemical bonds or hydrogen bonds were formed to reverse the surface potential of nanoparticles to positive, thus achieving the purpose of modification. In addition, other groups in the polymer chain might undergo addition or dehydration reactions with the hydroxyl groups, which could also be adsorbed on the surface of nanoparticles.

The surface potential of aramid fiber was negative in a neutral environment, therefore the nano-Al_2O_3 with positive surface could be organically bonded to the aramid matrix through electrostatic attraction, and the rest of the long chain had lipophilic groups which would weaken the difference between inorganic powders and organic polymers. In addition, the viscosity of the aramid fiber could increase the interfacial bonding force between the filler and the matrix, thereby improving the interfacial properties of the composite material.

Figure 4 The scheme of PDDA modification

(4) SEM

The cross sections of the aramid nanocomposite insulating paper filled with P-Al_2O_3 were characterized by SEM, and the effect of PDDA modification on the filler dispersion was analyzed. The cross-section SEM images of different samples were shown in Fig. 5. The filler in P-0 exhibited agglomeration phenomenon and the particle size was larger after PDDA modification. The overall particle size of the filler shown in Fig. 5(b) became smaller, and the dispersion was more uniform, indicating that PDDA

modification could effectively prevent the agglomeration of nanoparticles and improved its dispersion in the aramid fiber matrix. In Fig. 5(c), PDDA acted as a "flocculant" when the amount of modifier continued to increase, resulting in the fillers re-agglomeration and a decrease in the modification effect. In Fig. 5(d), when the amount of filler increases, the PDDA modified layer fell off during the papermaking process, and the electrostatic repulsion between the fillers decreased and agglomeration occurred again.

Figure 5 The section SEM images of (a)P-0, (b)P-10, (c)P-80, (d)P-10/7

(5) TG test:

The normalized TG and DTG curves were shown in Fig. 6(a)-(b) respectively. The decomposition rate of the sample was obviously accelerated at 400 ~ 600 ℃. The ash ratio was used to reflect the residues of filler and undecomposed PMIA. The ash residue of the samples after adding PDDA was slightly higher than that of the unmodified ones, indicating that the modification had a delaying effect on the decomposition of the matrix. The decomposition peaks of PDDA appeared at 345 ℃ and 455 ℃, and the corresponding decomposition peaks appeared in the vicinity of the modified composite paper, indicating that PDDA was successfully integrated into the composite system. In addition, the composite paper decomposition peaks appeared at 436 ℃ and 516 ℃, while the corresponding peaks shifted to the right for the modified samples, indicating that PDDA could delay the matrix decomposition.

Figure 6 the (a) TG and (b) DTG curves of composite samples

3.2 | Conductivity Properties

The conductivity was measured by Geely 6514 galvanometer and HPPS0619 high-power DC power. the experiment was tested by three-electrode measurement according to the method of measuring the volume resistivity of insulating paint film, as shown in Fig. 7(a). the measuring electrode was connected to the electrometer and the high-voltage electrode was connected to the DC power supply through the protection resistor. The whole platform was encapsulated in a stainless steel shielding cavity. the conductivity was tested under 1.8 kV DC voltage for 3 min to stabilize before reading the conductivity current from the electrometer. In order to reduce the influence of residual charge on the test, electrostatic cloth was used to discharge the surface of the paper sample after each test, and then stand on the grounding table for 5 min.

The electrical conductivity of the aramid insulating paper calculated by formula (1) was shown as Fig. 7(b).

$$\sigma_v = \frac{L}{\pi r^2} \cdot \frac{I_v}{U}$$

1

Where, L was the thickness of the sample, I_V was the conductance current, r was the radius of the test electrode, U was the applied voltage and takes 1.8 kV. Each sample was tested 10 times and the average value was used for analysis.

The bulk conductivity of P-0 was 1.12×10^{-16} S/m. With the increase of PDDA concentration, the bulk conductivity first decreased and then increased in the saturation state. When the PDDA mass fraction was 10%, the minimum volume conductivity was 3.62×10^{-17} S/m, which decreased 68% relative to P-0, and the bulk conductivity of P series was lower than that of pure Al_2O_3/aramid composites. According to the "multi-core model",[31] as a coupling agent, PDDA could provide the polymer chains and functional groups required for the bonding layer, enhance the bonding between nanoparticles and the matrix, effectively inhibit the migration of carriers in the composite material and reduce its bulk conductivity. However, as a strong electrolyte, it would provide carriers and lead to an increase in conductivity when the amount of PDDA was too high. With the increase of the doped nano-Al_2O_3 concentration, the conductivity of the insulating paper first decreased and then increased. When the doping concentration was 3%, it had the smallest conductivity, and when the doping concentration was 1% the conductivity decreased by 53%. Since Al_2O_3 had good insulating properties and its trace doping could destroy the carrier channels inside the PMIA matrix, the interface between the matrix and the nano-filler had an "electric double layer" structure,[32] and the conductivity of the electric double layer was higher than that of the polymer. Therefore, as the amount of filler continued to increase, the particle spacing in the polymer decreased, so that the electric double layers of adjacent particles would overlap, and the electrical conductivity of the overlapping region would increase significantly, which in turn affected the charge transport mechanism of the entire polymer. Combined with the electrical conductivity characteristics introduced above, it was found that the breakdown strength of aramid paper was very consistent with the change trend of volume conductivity, and the two were negatively correlated. Therfore, it could be considered that the charge transport ability of the polymer was an important factor affecting the breakdown performance.

Figure 7 (a)The volume conductivity platform. (b)The result of volume conductivity

3.3 | Breakdown Properties

The column-column electrode was used for testing breakdown strength, as shown in Fig. 8(a). The upper and lower electrodes were brass, and the diameter and height of the column electrode were 25 mm. The chamfering radius was 3 mm. During the test, a positive AC voltage was applied to the sample, and the breakdown strength of the aramid insulating paper under air conditions was measured by the method of continuous and uniform voltage increased as 2 kV/s. Each sample was tested 10 times on different parts to obtain the breakdown voltage, the thickness of the paper sample at the corresponding position was measured, and the average breakdown strength was calculated.

The Weibull distribution was widely utilized to describe the phenomenon of overall failure of insulation properties. In order to make the results more reasonable. Two-parameter Weibull model was used for analyzing. The cumulative probability function was shown as follows:

$$Pv = 1 - \exp[-(\frac{V}{\alpha})^{\beta}]$$

2

Where, V was the breakdown voltage. Pv was the breakdown failure. α and β were the paper scale and shape parameter, and indicated the breakdown voltage at the probability of 63.2% and the stability of the sample.

The AC breakdown strength of the aramid paper was shown in Fig. 8(b). The value Pv with a breakdown probability of 63.2% was extracted for comparison. It could be seen that the α of P-0 was 32.7 kV/mm. With the increase of PDDA concentration, the breakdown field strength of the aramid nanocomposite insulating paper showed a trend of increasing, then decreasing, and then increasing. When the mass fraction of modifier was 10%, the highest was 39.3 kV/mm, which was 20% higher than that when unmodified Al_2O_3 was doped. Continuing to increase the content of modifier, it was still higher than without modification. The average breakdown field strength of PMIA doped with different concentrations of P-10 first increased and then decreased with increasing doping concentration in a "V" pattern. The α of P-10/1 was 26.5 kV/mm, which was 48% lower than P-10/3. The breakdown field strengths of other doping concentration papers were lower than that of P-0, and the modification effect was poor, indicating that the concentration of nano-filler was higher than that of the modifier. The impact on the breakdown strength of the aramid paper was more significant.

Due to the strong cohesion of nano-powder, it is easy to agglomerate in aqueous solution, and the particle size increases after agglomeration, which is unable to give full play to the excellent properties of nanomaterials. Adsorption of positively charged PDDA on the surface of nano-Al_2O_3 by electrostatic attraction could increase the absolute value of its surface Zeta potential, which could increase the electrostatic repulsion between Al_2O_3 particles, prevent their aggregation, leading to the stably suspension and uniformly dispersion in the aramid matrix during the paper preparation process. In addition, PDDA had good dissociation ability in a wide pH range. In ethanol/water mixed solution, Cl^- and positively charged polymer chain could be dissociated, and the polymer chain with NH_3 functional group could form N-containing hydrogen bond with the aramid fiber matrix, enhancing the bonding of Al_2O_3 to the matrix interface. When the amount of PDDA was slightly increased, PDDA could form spherical micelles, which formed a sufficient coating layer on the surface of Al_2O_3, and the particle size of nanoparticles was significantly reduced based on the theory of "adsorption and electric neutralization" of the polymer[33]. At the same time, the increased PDDA would provide more N elements to generate hydrogen bonds with the matrix. When the concentration was too high, the modified layer would fall off, resulting in less repulsive than attractive force between the fillers, and the agglomeration phenomenon would reappear, destroying the interface characteristics between the filler and the matrix.

Figure 8 (a)Breakdown voltage test platform. The Weibull result of breakdown strength tests of (b) P series and (c) P-10 series.

3.4 | Trap Properties

In this paper, a self-made shielding cavity was used to measure the surface charge dissipation of aramid insulating paper. The device was shown in Fig. 9(a). The equipments include: Trek 347 electrometer from TREK company in the United States, with a measuring range of 0 ~ ± 3 kV; LAS60300P high-voltage power supply produced by Boer High Voltage Power Co., Ltd., which output voltage was adjustable from 0 to 100 kV. In the test, the surface of the paper sample was first treated with electrical discharge with a conductive cloth, and the surface potential of the grounding plate was measured to determine the initial potential of 0. After heating the grounded stage to 60 ℃, the sample was placed on the stage to preheat for 5 min. The needle electrode was used to apply 5 kV positive DC voltage at 5 mm above the paper sample for charging for 2 min. After charging, the paper sample was moved to 2 mm below the capacitance probe to monitor the surface potential, and the potential decay signal was continuously collected within 10 minutes through the data acquisition card (NI USB-8452).

There were two main ways of charge dissipation charge on the surface of the insulating paper: transfer into the body and dissipate along the surface of the paper.[34] The surface potential dissipation curves of the aramid paper were shown in Fig. 9(b) and 9(c). It could be seen from the figures that the dissipation trend of all samples were first fast and then slow. The initial potential of the composite material increased first, then decreased, and then increased again with the increase of PDDA mass fraction, and first increase and then decrease with the increase of Al_2O_3 doping concentration, the change trend of the decay rate was opposite to that of the initial surface potential, showing a good synergistic effect. As the dosage of PDDA increased, its excellent dissociation ability would provide more charge and conduction channels, and the dissipation rate would increase. Al_2O_3 possessed excellent insulating properties and high dielectric constant. The greater the dielectric barrier height, the more difficult it was to inject charges into the dielectric body. The greater the accumulation of charge on the dielectric surface, the slower the dissipation rate. The micro-doped Al_2O_3 could give full play to its good insulating properties and effectively hinder the transfer of charge to the interior of the matrix. A large number of conductive channels were formed between the excess fillers and the charges could migrate and the rate of dissipation began to increase again. It could be seen from the figure that the overall dissipation rate of P-10 series was higher than that of P series, indicating that PDDA and Al_2O_3 would provide different conductive channels. The impact on composite materials was a process of trade-offs, and they must cooperate with each other for a better overall effect.

Since aramid paper was made of fibers with different structures bonded together through physical processes, there were many large physical pores and chemical impurities randomly distributed within its interior due to the randomness and inhomogeneity nature of the dispersion. The defects introduced localized or local energy state into the energy gap of the polymer, and these trapping energy levels could trap carriers, reducing their mean free path and then the accumulated energy. These structures present in polymers capable of trapping charges were defined as "traps".[35] The trapped charges couldn’t be neutralized from each other through recombination, and the internal electric field formed by them would

affected the breakdown, aging and flashover characteristics of the dielectric under high field strength.[36] According to the isothermal surface potential decay method(ISPD),[37] Trap properties could be described by the trap density I(t) and the trap depth E_T. I(t) and E_T were obtained by Eqs. (2) and (3).

$$I(T) = (\varepsilon_0 \varepsilon_r / eL) \cdot tdU / dT$$

3

$$E_T = k_B T \ln(vt)$$

4

Where, ε_0 was the vacuum permittivity, ε_r was the relative permittivity, e was the elementary charge, L was the thickness of the paper sample, dU/dT was the decay rate of the surface potential, k_B was the Boltzmann constant, T was the temperature, v was the charge escape frequency, here the low frequency field was 4.17×1013 s^{-1}.

The trap distribution curves of the composites insulating material calculated by formula (2) and (3) were shown in Fig. 9(d) and 9(e). It could be seen that P-0 had both deep and shallow traps. The depth of shallow trap was 0.932 eV, and the energy center of deep trap level was 1.015 eV. After PDDA modification, the depth and density of the aramid paper traps were improved, the shallow traps of P-10 disappeared, and the depth of the deep traps was 1.040 eV at most. It could be obtained that the interface properties between the modified Al_2O_3 and the aramid matrix were improved. With the continuous increase of PDDA amount, the depth and density of the traps showed a saturated decreasing trend, and the shallow traps tended to reappear, indicating that excessive use of PDDA would introduce new physical defects and chemical impurities, changing the structure of deep traps or introduce shallow traps. With the increase of Al_2O_3 content, the depth and density of traps first increased and then decreased, and both were dominated by deep traps, confirming that the combination effect of aramid fiber and filler was better when the mass fraction of PDDA was 10%; When the filler content was 7%, shallow traps reappeared, and the density of deep traps decreased. The reason might be that too many composite nano-fillers can cause secondary agglomeration, resulting in an increase in the particle size and specific surface area of the filler. Therefore, it couldn't be closely combined with the matrix, introducing more defects and interface problems, resulting in deep traps shallower. The breakdown strength of aramid nanocomposites had a very similar trend to the depth and density of deep traps, and it could be considered that deep trap was another important factor affecting the breakdown properties.

Figure 9 (a)Charge dissipation test platform. (b)(c)The surface potential dissipation. (d)(e)The trap distribution of PMIA.

Table 2 The trap distribution of samples

Table 2
The trap distribution of samples

Item	Swallow trap(eV)	Deep trap(eV)
P-0	0.932	1.015
P-10	none	1.040
P-20	0.929	1.016
P-40	0.920	1.019
P-80	0.920	1.020
P-10/1	0.926	1.033
P-10/5	0.920	1.037
P-10/7	0.932	1.040

3.5 | Molecular Dynamics Simulation

Aramid paper is composed of chopped fibers and precipitated fibers with the same structural formula. They are zigzag long molecular chains obtained by the polymerization of isophthalic acid and m-phenylenediamine as monomers with the chemical formula of $(C_{14}H_{10}N_2)_n$. Aramid fibers exist in two states in the paper: crystalline and amorphous region. The molecules in the crystalline region are compact and ordered, while the molecules in the amorphous region are irregularly distributed and has larger air strikes and smaller intramolecular and intermolecular forces. The crystallinity of PMIA is about only 20%~30%. Therefore, this paper only considered the construction of aramid amorphous structure, and all the simulations were carried out in the non-unit cell model in Accelrys Materials Studio (MS) software. Firstly, a PMIA amorphous box with a density of 1.3 g/cm^3, a force field of COMPASS II, and a single molecular chain length of 10 was built using the Amorphous Cell module.[38] The alumina supercell was imported from the "Building" module database to form nanostructures, and the (012) section of the unit cell with a cutting thickness of 25 Å was selected for the study because this section exposed all types of O and Al elements. The PDDA molecular chain was built in building model. PMIA□Al_2O_3 and PDDA models were shown in Fig. 10(a)(b)(c), respectively.

The interface model between aramid fiber and aluminum dioxide using the Build layer was shown in Fig. 10(c). Since the two materials were periodically distributed in the simulation setting, the thickness of the vacuum layer was set to 50 Å to prevent the influence of adjacent materials. Based on the above model, PDDA was introduced into the interface with a trans structure and DP of 1, as shown in Fig. 10(d).

After the model was built, structurally optimization was needed to make it more reasonable. The optimization step was 200,000 to ensure that the most stable and approximate structure of the real material was achieved.[39] The stable working temperature of aramid paper is about 453 K. Hence, 298 ~ 448 K was chosen as the simulation temperature range, and 4 certain temperatures with 50 K as the step

for NVT dynamics simulation, adopting Andersen temperature control method. The total time step was 500 ps, each step was 1 fs, and the dynamic characteristics of each atom in the system were collected every 5000 ps for subsequent analysis. The initial velocity followed the Boltzmann distribution, the external pressure was standard atmospheric pressure, and the Berendsen method was used for control. Electrostatic interaction and van der Waals function were adjusted by Ewald and Atom based method, respectively, and the Drieding force field was used for both structural optimization and dynamic simulation.

In nanocomposites, the interface accounts for a high-volume fraction, and the interface properties has a very important influence on the physical and chemical properties of the composites. The interfacial binding energy is often used to indicate the strength of intermolecular interactions in polymers. The larger the absolute value, the more energy required to break the interface and the more stable the structure. The definition is as follows:

$$E_{\text{int } eraction} = E_{total} - E_1 - E_2$$

4

Where, $E_{interaction}$ was the interface binding energy, E_{total} was the overall energy, E_1 was the energy possessed by PMIA, E_2 was the energy possessed by the alumina crystal plane.

The interfacial binding energies of the model before and after modification at different temperatures were shown in Fig. 10(e). With the increase of the simulation temperature, the models before and after modification showed a saturated increasing trend, and the increase rate was fast at first and then slow. The main reason was that when the temperature was low, a large number of hydrogen bonds could be formed between the interfaces, while high temperature would hinder the generation of hydrogen bonds. It could be clearly found that the interface binding energy of the modified model was significantly improved at different temperatures than before the modification, which was because PDDA could introduce N atoms to form NH…O hydrogen bonds and enhance the interaction between the components, thereby improving the dielectric properties of the composite material.

Figure 10 (a)PMIA, (b)Al_2O_3, (c)PDDA. PMIA/Al_2O_3 models of the (d) unmodified and (e) modified with PDDA. (f)Interaction energy of unmodified and modified PMIA/ Al_2O_3

4 Conclusion

In this paper, PDDA was successfully coated on the surface of nano-Al_2O_3 by electrostatic interaction and the modified nano-Al_2O_3 exhibited great dispersity in the aramid fiber matrix. The effect of PDDA fraction and filler content was carefully studied and optimized formula was achieved. Satisfactory improvement in insulation performance and breakdown strength was observed for Al_2O_3/PMIA composite paper. Moreover, the effect mechanism of PDDA on the electrical properties of Al_2O_3/PMIA composite insulating

paper was studied. PDDA can increase the electrostatic repulsion between nano-Al_2O_3 particles, which is conducive to the dispersion of fillers in the composite matrix; in addition, the introduction of PDDA reduced the interfacial binding energy of alumina and aramid, and improved the interfacial binding force between fillers and matrix. In conclusion, we believe this reserch can provide both theoretical support and practical guide for the development of high-performance insulation composites.

Declarations

ACKNOWLEDGENTS

This study was supported by The National Natural Science Foundation of China (51777076) and The Research Project of State Key Laboratory (LAPS-202103)

Funding

This work was supported by The National Natural Science Foundation of China (51777076) and The Research Project of State Key Laboratory (LAPS-202103)

Competing Interests

The authors have no relevant financial or non-financial interests to disclose.

Author Contributions

All authors contributed to the study conception and design. Material preparation, data collection and analysis were performed by Lu Xiuquan, Song Jingxuan and Zhu Meiying. The first draft of the manuscript was written by Lu Xiuquan and all authors commented on previous versions of the manuscript. All authors read and approved the final manuscript.

References

1. M. Grujicic, W.C. Bell, P.S. Glomski, B. Pandurangan, C.F. Yan, B.A. Cheeseman. Filament-Level Modeling of Aramid-Based High-Performance Structural Materials. J. Mater. Eng. Perform, 20(8): 1401–1413(2011). DOI: 10.1007/s11665-010-9786-y.
2. M.Z. Li, K. Cheng, C.H. Wang, S.J. Lu, Functionaliza aramid fibers with polydopamine to possess UV resistance. J. Inorg. Organomet. Polym. Mater. 31(7), 2791-2805 (2021). DOI: 10.1007/s10904-021-01910-9.
3. F. Suarez-Garcia, S. Villar-Rodil, C.G. Blanco, A. Martinez-Alonso, J. Tascon. Effect of Phosphoric Acid on Chemical Transformations during Nomex Pyrolysis. Chem. Mater. 16(13): 2639-2647 (2004). DOI: 10.1021/cm0349654.
4. F. Yin, C. Tang, Y.J. Tang, Y.G. Gui, Z.Y. Zhao, Reactive molecular Dynamics Study of Effects of Small-Molecule Organic Acids on PMIA Thermal Decomposition. J. Phys. Chem. B. 122(45): 10384-10392

(2018). DOI:10.1021/acs.jpcb.8b09343.

5. M.L. Wu, L. Ding, J. Liao, Y. Zhang, W.K. Zhu. Preparation of novel porous Al_2O_3-SiO_2 nanocomposites via solution-freeze-drying-calcination method for the efficient removal of uranium in solution. Nanotechnology. 33(9): 095705 (2021). DOI: 10.1088/1361-6528/ac3c7a.
6. Y.X. Mai, B. Du, Q. Liu, W. Zhao, B.Y. Yan. Influence of Micro@Nano-Al_2O_3 Structure on Mechanical Properties, Thermal Conductivity, and Electrical Properties of Epoxy Resin Composites. J. Electron. Mater. 51: 232–242 (2022). DOI:10.1007/s11664-021-09283-y.
7. X. Yang, Z.H. Jiang , W.D. Li, C. Wang, M.Y. Chen, G.J. Zhang. The role of interfacial H-bonding on the electrical properties of UV-cured resin filled with hydroxylated Al_2O_3 nanoparticles. Nanotechnology. 31(27): 275710 (2020). DOI: 10.1088/1361-6528/ab824f.
8. N. El-Atab, T.G. Ulusoy, A. Ghobadi, J. Suh, R. Islam, A.K. Okyay, K. Saraswat, A. Nayfeh. Cubic-phase zirconia nano-island growth using atomic layer deposition and application in low-power charge-trapping nonvolatile-memory devices. Nanotechnology. 28(44): 445201 (2017). DOI: 10.1088/1361-6528/aa87e5.
9. M.Z. Khan, A. Waleed, A. Khan, M. Hassan, Z.J. Paracha, H. Farooq. Significantly Improved Surface Flashover Characteristics of Epoxy Resin/Al_2O_3 Nanocomposites in Air, Vacuum and SF_6 by Gas-Phase Fluorination. J. Electronic. Mater. 49(5): 3400–3408 (2020). DOI: 10.1007/s11664-020-08001-4.
10. E.M. Abou Hussein, N.A. El-Alaily, Study on the Effect of Gamma Radiation on Some Spectroscopic and Electrical Properties of Lithium Borate Glasses. J. Inorg. Organomet. Polym. Mater. 28(3), 1214-1225 (2018). DOI: 10.1007/s10904-017-0776-5.
11. J. Yu, G. Wang, R. Huo, C. Wu, X. Wu, P. Jiang. Influence of interface structure on dielectric properties of epoxy/alumina nanocomposites. Macromol. Res. 20(8): 816–826 (2012). DOI: 10.1007/s13233-012-0122-2.
12. B.H. Fan, D.L. He, Y. Liu, J.B. Bai. Influence of Thermal Treatments on the Evolution of Conductive Paths in Carbon Nanotube-Al_2O_3 Hybrid Reinforced Epoxy Composites. Langmuir. 33 (38): 9680-9686(2017). DOI: 10.1021/acs.langmuir.6b03915.
13. I.L.M. Costa, N.C. Zanini, D.R. Mulinari. Thermal and Mechanical Properties of HDPE Reinforced with Al_2O_3 Nanoparticles Processed by Thermokinectic Mixer. J. Inorg. Organomet. Polym. Mater. 31(1), 220-228 (2021). DOI: 10.1007/s10904-020-01709-0
14. S.S. Kumar, G. Kanagaraj. Investigation of Characterization and Mechanical Performances of Al2O3 and SiC Reinforced PA6 Hybrid Composites. J. Inorg. Organomet. Polym. Mater. 26(4), 788-798 (2016). DOI: 10.1007/s10904-016-0387-6
15. X.Y. Ma, L.Z. Liu, H.J. He, L. Wang. Effects of interface bonding on the corona resistance of the polyimide/nano-Al_2O_3 three-layer composite films. High. Perform. Polym. 30(10): 1240-1246 (2018). DOI: 10.1177/0954008317746474.

16. Z. Ghezelbash, D. Ashouri, S. Mousavian, A.H. Ghandi, and Y. Rahnama. Surface modified Al_2O_3 in fluorinated polyimide/Al_2O_3 nanocomposites: synthesis and characterization. Bull. Mater. Sci. 35(6): 925-931(2012). DOI: 10.1007/s12034-012-0385-4.
17. L.H. Wang, F. Yin, Y. Shen, C. Tang. Reactive molecular dynamics research on influences of water on aging characteristics of PMIA insulation paper. J. Appl. Phys. 127(10): 105107 (2020). DOI: 10.1063/1.5129314.
18. J.F. Zhang, Q.G. Chen, M.H. Chi, H.D. Yang, H.Q. Liu. Space charge and insulation properties of nano-Al_2O_3-modified oil-impregnated paper used for HVDC convertor transformer. J. Mater. Sci. Mater. Elect. 32(3): 3720–3731(2021). DOI:10.1007/s10854-020-05117-5.
19. N.C. Liang, R.J. Liao, M. Xiang, Y. Mo, Y. Yuan. Effect of Nano Al_2O_3 Doping on Thermal Aging Properties of Oil-Paper Insulation. Energies. 11(5): 1176 (2018). DOI: 10.3390/en11051176.
20. H.O. Ruan, Q. Xie, S.S. Wang, Y.H. Zhang, J.X. Song, Q.J. Duan, F.C. Lv. Experimental Study on Damage Mechanism of Partial Discharge of Oil-Immersed Laminated PMIA Paper. IEEE T Dielect El In. 28(4): 1223–1230 (2021). DOI: 10.1109/tdei.2021.009548.
21. C. Du, C.R. Liu, X. Yin, H.C. Zhao, Synthesis and Bonding Performance of Conductive Polymer Containing Rare Earth Oxides. J. Inorg. Organomet. Polym. Mater. 28(3), 746-750 (2018). DOI: 10.1007/s10904-017-0713-7
22. B. Zhang, T.Z. Liang, X.M. Shao, M. Tian, N.Y. Ning, L.Q. Zhang, W.C. Wang. Nondestructive Grafting of ZnO on the Surface of Aramid Fibers Followed by Silane Grafting to Improve its Interfaceal Adhesion Property with Rubber. ACS. Appl. Polym. Mater. 3(9): 4587-4594 (2021). DOI: 10.1021/acsapm.1c00682.
23. X.Y. Huang, P.K. Jiang, Y. Yin. Nanoparticle surface modification induced space charge suppression in linear low density polyethylene. Appl. Phys. Lett. 95(24): 242905 (2009). DOI: 10.1063/1.3275732.
24. L. Zhang, Y.X. Zhou, X.Y. Cui, Y.C. Sha, T.H. Le, Q. Ye, J.H. Tian. Effect of nanoparticle surface modification on breakdown and space charge behavior of XLPE/SiO_2 nanocomposites. IEEE T Dielect El In. 21(4): 1554–1564 (2014). DOI: 10.1109/tdei.2014.004361.
25. S.H. Wang, P.X. Chen, S.H. Yu. P. Zhang, J.Y. Li, S.T. Li. Nanoparticle dispersion and distribution in XLPE and the related DC insulation performance. IEEE T Dielect El In. 25(6): 2349–2357 (2018,). DOI: 10.1109/tdei.2018.007156.
26. K. Kan, D. Moritoh, Y. Matsumoto, K. Masuda, M. Othtani, K. Kobiro. Nanoscale Effect of Zirconia Filler Surface on Mechanical Tensile Strength of Polymer Composites. Nanoscale. Res. Lett. 15(1): 51 (2020). DOI: 10.1186/s11671-020-3282-6.
27. R.P. Bagwe, L.R. Hilliard, W.H. Tan. Surface Modification of Silica Nanoparticles to Reduce Aggregation and Nonspecific Binding. Langmuir. 22(9): 4357–4362 (2006). DOI: 10.1021/la052797j.
28. F.Y. Li, Q.Y. Yang, F. Qiu, Y. Liu. Modification of superparamagnetic iron oxide nanoparticles with poly(diallyldimethylammonium chloride) at air atmosphere. Polym. Adv. Tech. 27(11): 1530–1534 (2016). DOI: 10.1002/pat.3834.

29. T. Ratajski, I. Kalemba-Rec, P. Indyka, P. Ledwig, M.J. Szczerba, B. Dubiel. Effect of PDDA surfactant on the microstructure and properties of electrodeposited SiO_2/Ni nanocomposites. Mater. Charact. 163: 110229 (2020). DOI: 10.1016/j.matchar.2020.110229.
30. I. Zhitomirsky. Electrochemical processing and characterization of nickel hydroxide–polyelectrolyte films. Mater. Lett. 58(3): 420-424 (2004). DOI: 10.1016/S0167-577X(03)00516-0.
31. T. Tanaka. Dielectric nanocomposites with insulating properties. IEEE T Dielect El In. 12(5): 914–928 (2005). DOI: 10.1109/tdei.2005.1522186.
32. T.J. Lewis. Interfaces are the dominant feature of dielectrics at the nanometric level. IEEE T Dielect El In. 11(5): 739-753(2004). DOI: 10.1109/TDEI.2004.1349779.
33. S.Y. Yoon, Y.L. Deng. flocculation and reflocculation of clay suspension by different polymer systems under turbulent conditions. J. Colloid. Int. Sci. 278(1): 139-145 (2004). DOI: 10.1016/j.jcis.2004.05.011.
34. J. Kindersberger, C. Lederle. Surface charge decay on insulators in air and sulfurhexafluorid-Part ⅱ Measurements. IEEE T Dielect El In. 15(4): 949-957 (2008). DOI: 10.1109/TDEI.2008.4591215.
35. T. Takada, Y. Hayase, Y. Tanaka, T. Okamoto. Space charge trapping in electrical potential well caused by permanent and induced dipoles for LDPE/MgO nanocomposite. IEEE T Dielect El In. 15(1): 152-160 (2008). DOI: 10.1109/T-DEI.2008.4446746.
36. M. Kumar, G.K. Vashistha, and Y.K. Sharmma. Single injection space-charge-limmited current in insulator with two sets of distributed traps. Eur. Phys. J. Appl. Phys. 40(2): 125-128 (2007). DOI: 10.1051/epjap:2007136.
37. W.W. Shen, H.B. Mu, G.J. Zhang, J.B. Deng, D.M. Tu. Identification of electron and hole trap based on isothermal surface potential decay model. J. Appl. Phys. 113(8): 083706 (2013). DOI: 10.1063/1.4792491.
38. C. Tang, S. Zhang, J.Y. Xie, C. Lv. Molecular simulation and experimental analysis of Al_2O_3-nanoparticle-modified insulation paper cellulose. IEEE T Dielect El In. 24(2): 1018–1026 (2017). DOI: 10.1109/tdei.2017.006315.
39. S. Urata, R. Ando, M. Ono, Y. Hayashi. Molecular dynamics study on nano-particles reinforced oxide glass. J. American. Ceram. Society. 101(6): 2266–2276 (2018). DOI: 10.1111/jace.15378.

Figures

Figure 1

preparation process of Al_2O_3/PMIA paper.

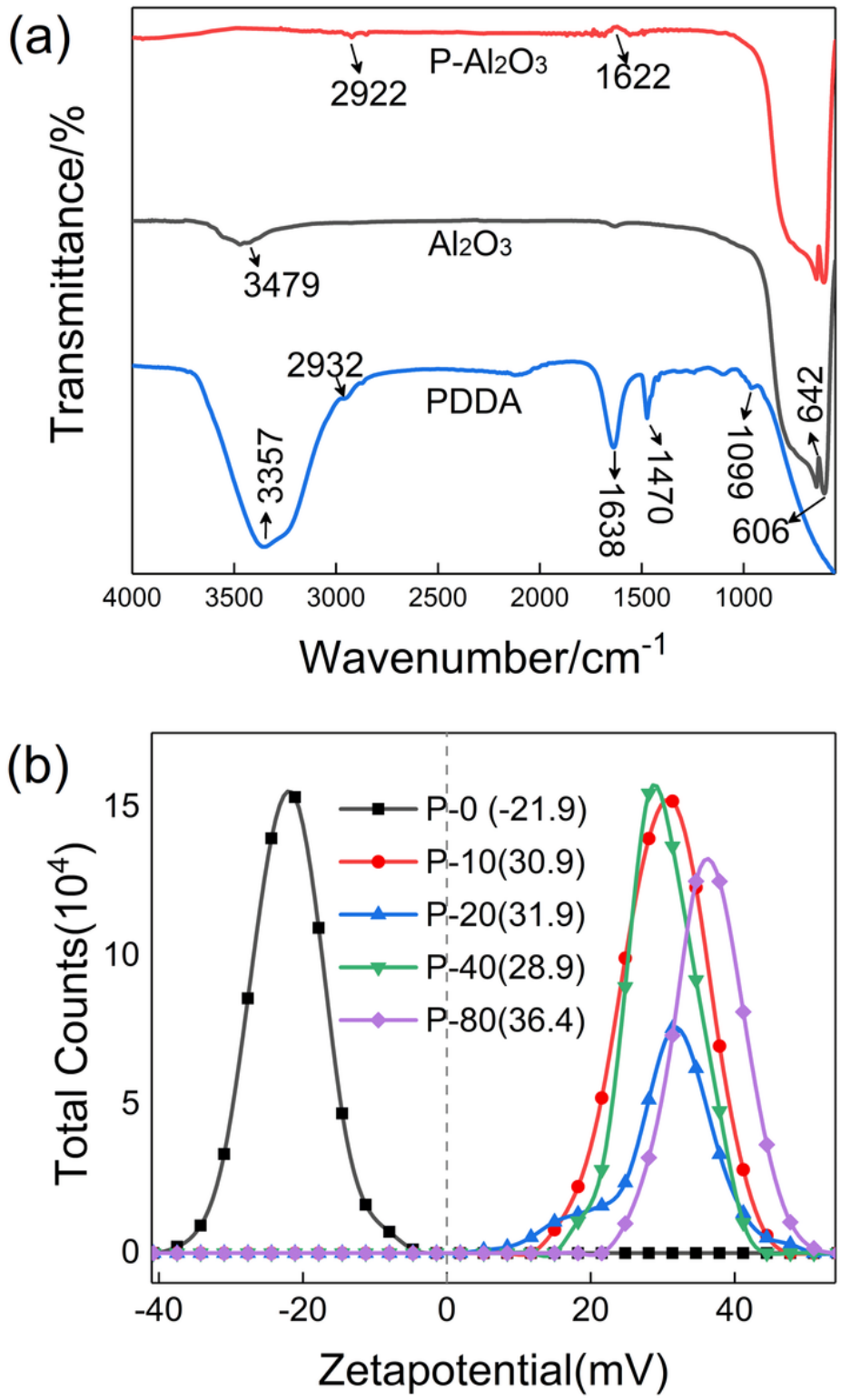

Figure 2

(a)FTIR comparion between PDDA, Al_2O_3 and PDDA/Al_2O_3 nanocomposites. (b)Particle zeta potential of nanocomposites with PDDA concentration.

Figure 3

The TEM images of (a)P-0, (b)P-10, (c)P-80.

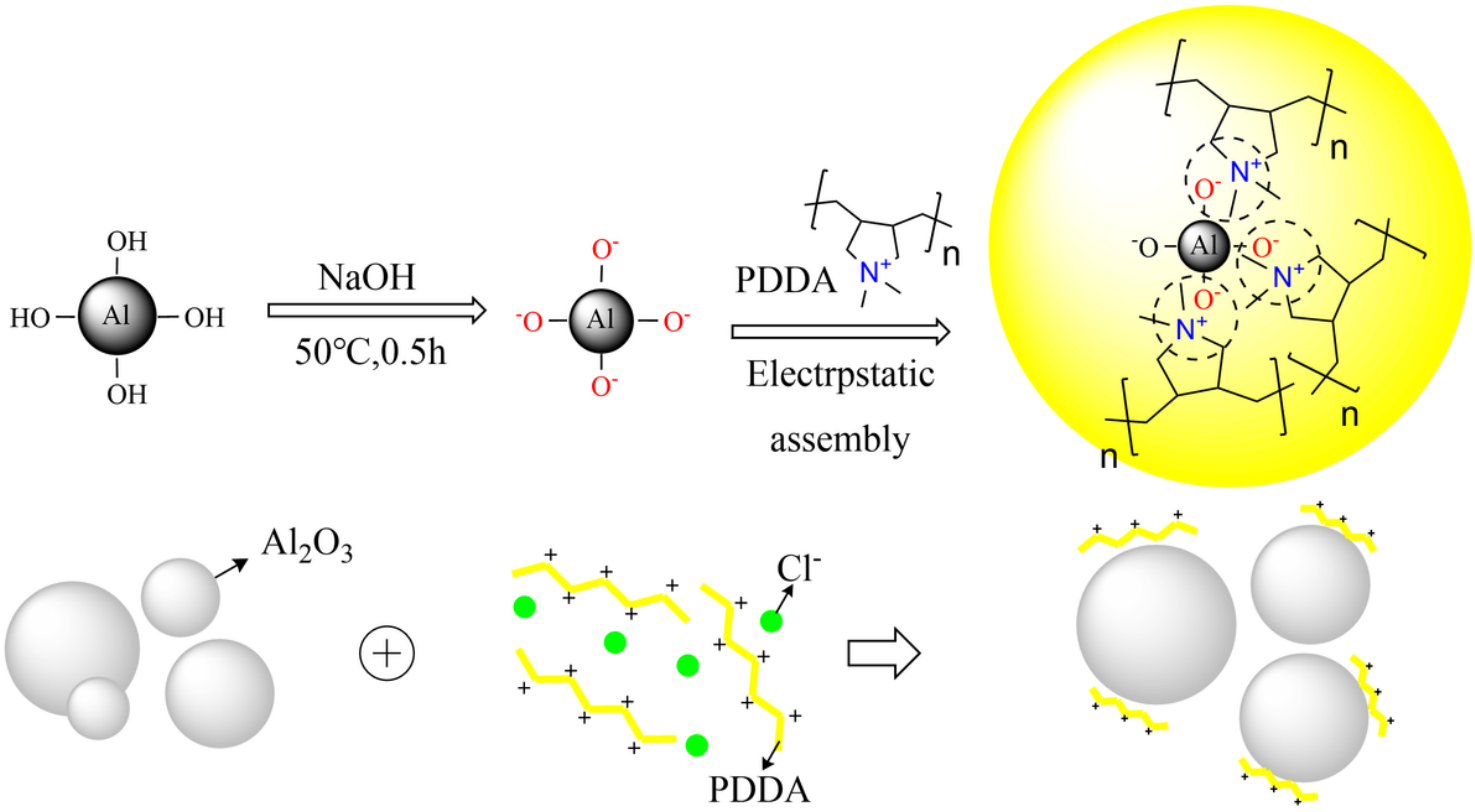

Figure 4

The scheme of PDDA modification.

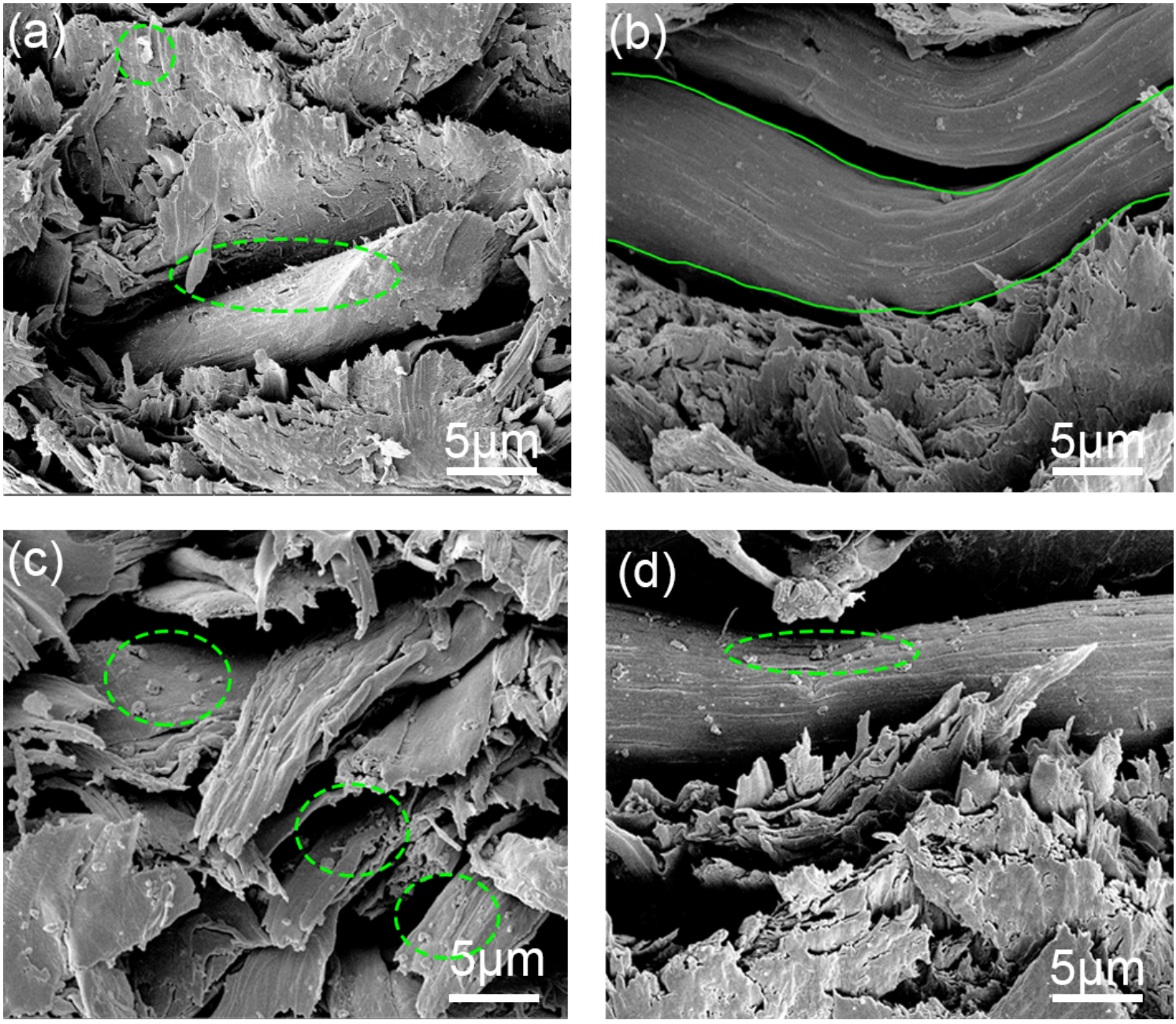

Figure 5

The section SEM images of (a)P-0, (b)P-10, (c)P-80, (d)P-10/7.

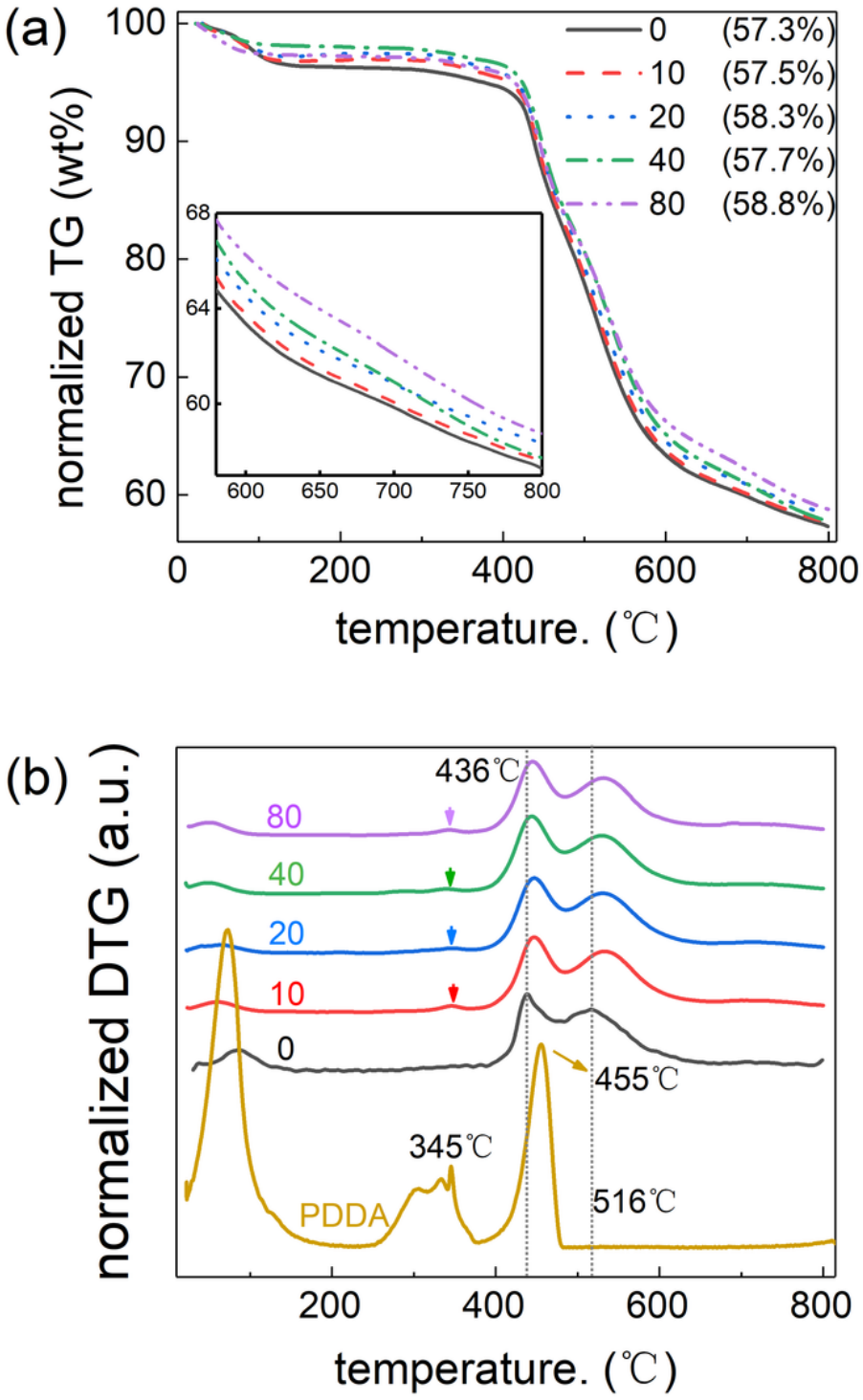

Figure 6

the (a) TG and. (b) DTG curves of composite samples.

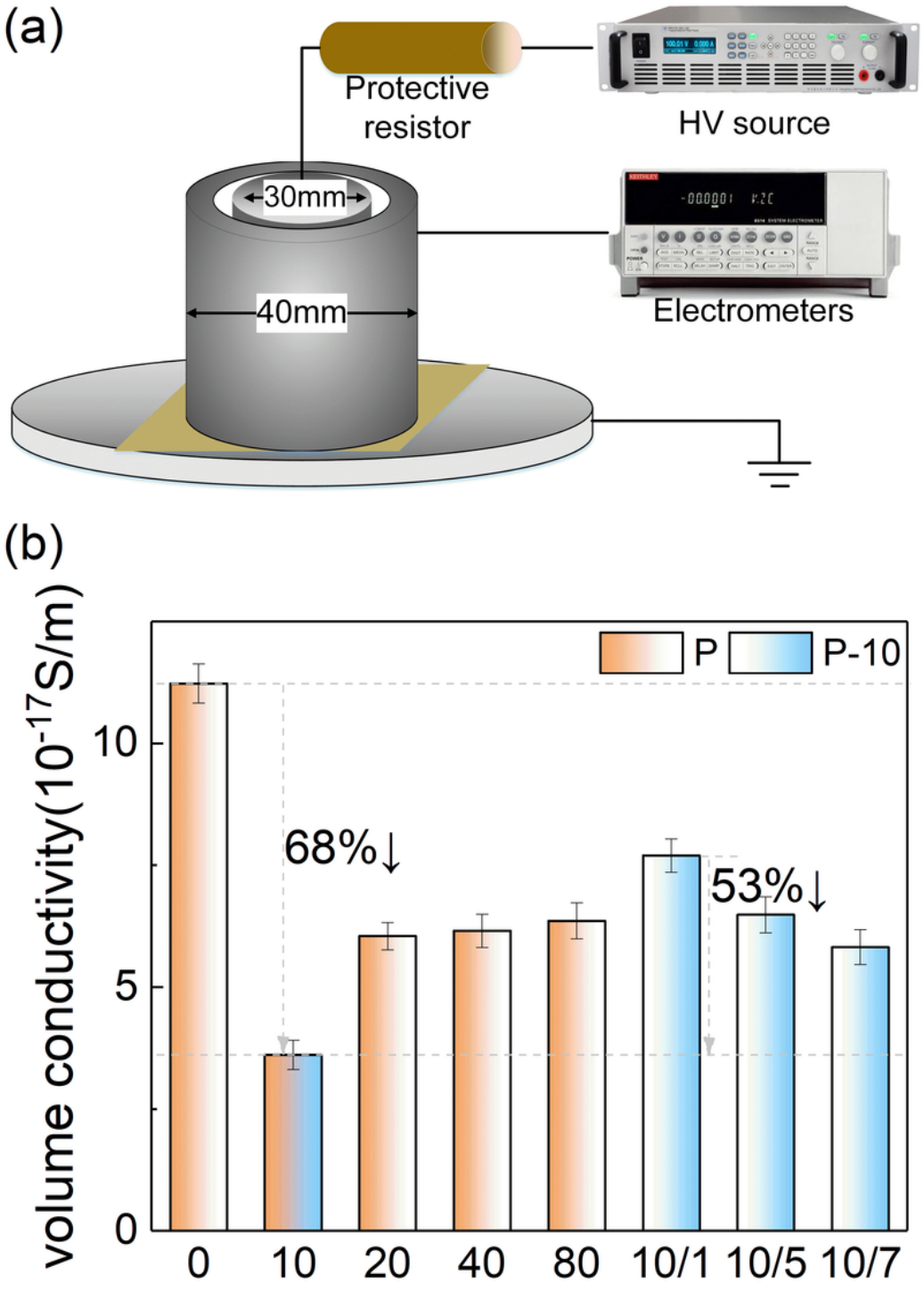

Figure 7

(a)The volume conductivity platform. (b)The result of volume conductivity.

Figure 8

(a)Breakdown voltage test platform. The Weibull result of breakdown strength tests of (b) P series and (c) P-10 series.

Figure 9

(a)Charge dissipation test platform. (b)(c) The surface potential dissipation. (d)(e) The trap distribution of PMIA.

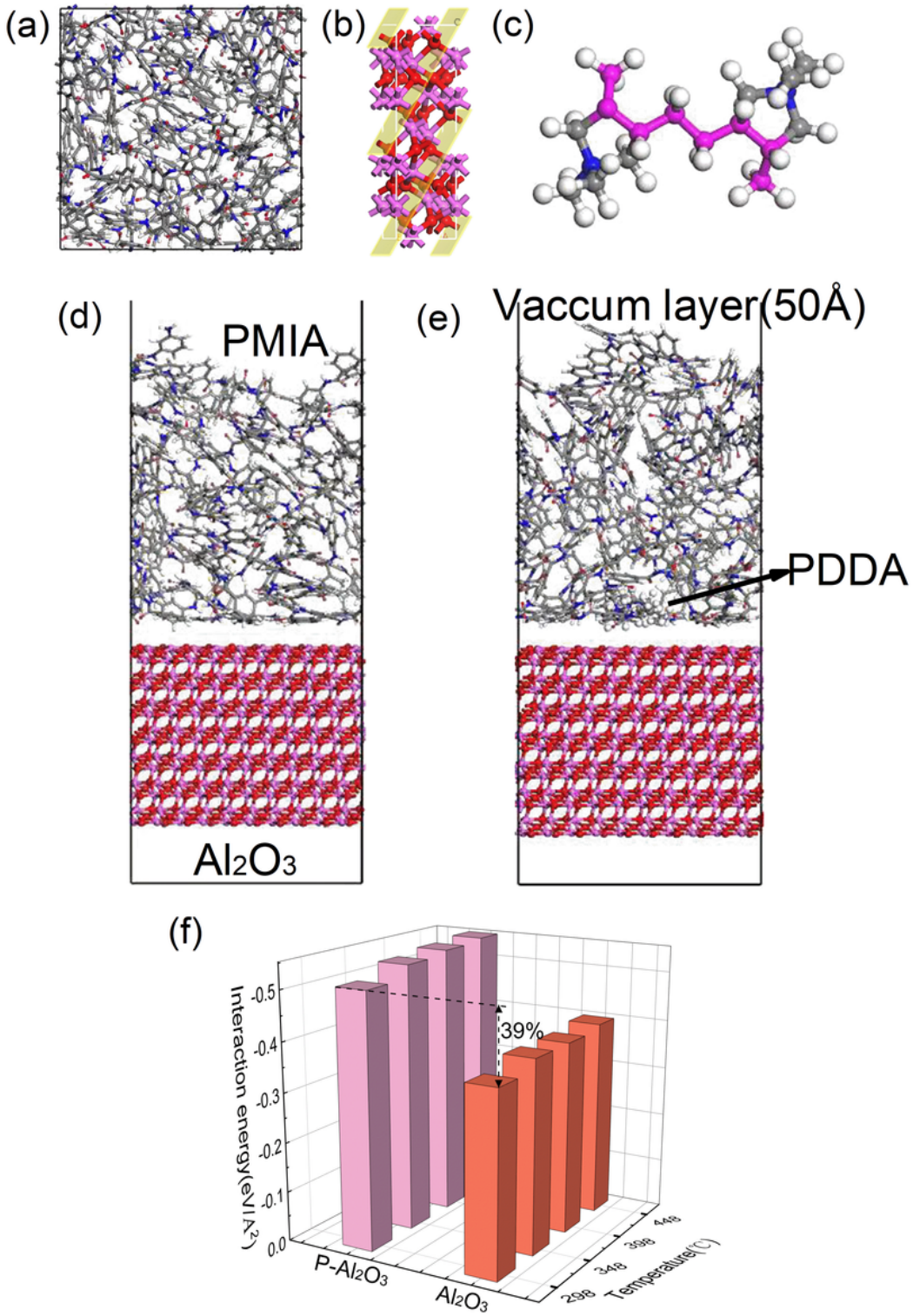

Figure 10

(a) PMIA, (b)Al_2O_3 (c)PDDA. PMIA/ Al_2O_3 models of the (b) unmodified and (c) modified with pdda. (d)Interaction energy of unmodified and modified PMIA/ Al_2O_3.